

Computation of bio-fluid sounds

Youngmin Bae and Young J. Moon*

Department of Mechanical Engineering, Korea University, Seoul, 136-701, Korea

Preprint submitted to International Journal of Aeroacoustics 18 June 2010

A hybrid method is proposed for prediction of bio-fluid sounds at very low Mach numbers. The unsteady hydrodynamic flow field is computed by the incompressible Navier-Stokes equations (INS), while the sound field is obtained by solving the linearized perturbed compressible equations (LPCE) with sound sources represented by a total derivative of the hydrodynamic pressure, DP/Dt . With the present INS/LPCE hybrid method, the vocal sound in human larynx and the buzz sound of bumblebee are computed with more clear understanding on the sound generation processes associated with their characteristic motions such as the self-sustained oscillatory motions of the vocal folds and the figure-eight motion of the flapping wings.

1. INTRODUCTION

A bio-fluid sound is the sound generated by fluid motions coupled with a biological body in motions; for example, phonation in human larynx, buzz sound of flapping wings, etc. Understanding of the bio-fluid sound is important not only for fundamental studies but also for its bio-mimetic applications. In many cases, however, sound generation processes are not fully understood yet.

In computational modeling of the bio-fluid sound, it is preferred that a method can predict the generation and propagation of the sound, considering the full geometry. Computational complexities come from the fact that in many cases, the problem is internal or external with a multi-body configuration. Therefore, an approach with acoustic analogy has been used but with a limited extent. Besides, the sound generation process often occurs at very low Mach number (e.g. less than Mach number 0.1). Difficulties are therefore associated with accurately resolving the weak compressibility effects. For many reasons, a direct numerical simulation (DNS) of flow and sound with the compressible Navier-Stokes equations is always an attractive tool but it becomes

numerically problematic at very low Mach numbers because a scale disparity between flow and acoustics is so large.

In this regard, we propose to use an INS/LPCE hybrid method [I] for bio-fluid sounds. The present hybrid method has been developed to predict the low-subsonic, turbulent flow noise related to the airframe noise, such as the trailing-edge noise, the forward-facing step noise, etc. The proposed INS/LPCE hybrid method is computationally efficient, especially at low Mach numbers because it is based on an incompressible flow solver and the grid systems for flow and acoustics can be treated differently. For example, turbulent flow field is computed by the incompressible large-eddy simulation (LES) with very high grid resolutions, while acoustic field can be obtained by solving the linearized perturbed compressible equations (LPCE), with noise sources represented by a total derivative of the hydrodynamic pressure, DP/Dt on a much coarse grid. With this grid-splitting technique, the time step restricted by a CFL condition can be largely relieved and thereby the afore-mentioned scale-disparity problem can be substantially reduced [1–3]. The stability and accuracy of the INS/LPCE method has been validated

for some benchmark problems, comparing with the DNS or analytical solution [1] as well as with the experimental data [4, 5].

The objectives of this study are (i) to show that the present INS/LPCE hybrid method can be extended further to predict the bio-fluid sounds of the human larynx and the bumblebee and (ii) to explain the sound generation processes more clearly with the underlying characteristic motions of the biological body, e.g. the vibrating motions of the vocal folds in human larynx and a figure-eight motion of the flapping wings of the bumblebee. Both cases are associated with very low Mach number aeroacoustics. In the former, the maximum jet speed of the puffed air through the vocal folds does not exceed Mach number 0.1 and in the latter, the maximum translational velocity of the wing is $M = 0.0485$. In section 2, computational methods for flow and acoustics are introduced. In section 3, flow and sound predicted by the present INS/LPCE hybrid method will be presented, with discussion on the noise sources and the noise generation mechanisms.

2. COMPUTATIONAL METHODOLOGIES

2.1. INS/LPCE SPLITTING METHOD

In the hydrodynamic/acoustic splitting method, the total flow variables are decomposed into the incompressible and perturbed compressible variables as,

$$\rho(\vec{x}, t) = \rho_0 + \rho'(\vec{x}, t) \quad (1)$$

$$\vec{u}(\vec{x}, t) = \vec{U}(\vec{x}, t) + \vec{u}'(\vec{x}, t) \quad (2)$$

$$p(\vec{x}, t) = P(\vec{x}, t) + p'(\vec{x}, t) \quad (3)$$

The incompressible variables of \vec{U} and P represent hydrodynamic flow field,

while acoustic fluctuations and other compressibility effects are resolved by perturbed quantities denoted by ($'$).

In the present study, the hydrodynamic flow field around the flapping wing is computationally modeled as a two-dimensional, incompressible, and laminar flow and computed by solving the incompressible Navier-Stokes equations (INS),

$$\nabla \cdot \vec{U} = 0 \quad (4)$$

$$\frac{\partial \vec{U}}{\partial t} + (\vec{U} \cdot \nabla) \vec{U} = -\frac{1}{\rho_0} \nabla P + \frac{\mu_0}{\rho_0} \nabla^2 \vec{U}, \quad (5)$$

where ρ_0 and μ_0 are constant values of density and dynamic viscosity of a fluid, respectively.

The corresponding sound field is then calculated by the linearized perturbed compressible equations (LPCE),

$$\frac{\partial \rho'}{\partial t} + (\vec{U} \cdot \nabla) \rho' + \rho_0 (\nabla \cdot \vec{u}') = 0 \quad (6)$$

$$\frac{\partial \vec{u}'}{\partial t} + \nabla(\vec{u}' \cdot \vec{U}) + \frac{1}{\rho_0} \nabla p' = 0 \quad (7)$$

$$\begin{aligned} \frac{\partial p'}{\partial t} + (\vec{U} \cdot \nabla) p' + \gamma P (\nabla \cdot \vec{u}') \\ + (\vec{u}' \cdot \nabla) P = -\frac{Dl}{D_i} \end{aligned} \quad (8)$$

where $DP/Dt = \partial P/\partial t + (\vec{U} \cdot \nabla)P$ and γ is the specific heat ratio.

The left hand sides of LPCE represent the effects of acoustic wave propagation and refraction in the unsteady, inhomogeneous flows, while the right hand side only contains the acoustic source term, which will be projected from the hydrodynamic solution. For very low Mach number flows, it is interesting to note that the total change of hydrodynamic pressure DP/Dt is considered as the only explicit

noise source term. The details of LPCE can be found in Reference [1].

Because a curl of the linearized perturbed momentum equations, Eq. (7) yields

$$\frac{\partial \bar{\omega}'}{\partial t} = 0, \quad (9)$$

the LPCE prevents any further changes (generation, convection, and decaying) of perturbed vorticity in time. In fact, the perturbed vorticity could generate self-excited errors, if $\bar{\omega}'$ is not properly resolved with the acoustic grid. Hence, the evolution of the perturbed vorticity is pre-suppressed in LPCE, deliberating the fact that the perturbed vorticity has little effects on noise generation, particularly at low Mach numbers. For hybrid methods [1], this is an important property that ensures consistent, grid-independent acoustic solutions. Derivation of LPCE and the detailed discussion on characteristics of the perturbed vorticity can be found in Reference [1].

In order to include the effects of moving geometry, the governing equations are solved in a moving coordinate system. The components of the transformation matrix between the physical space (x, y, t) and computational space (ξ, η, τ) are defined by

$$\begin{aligned} \xi_x &= \frac{y_\eta}{J}, \quad \xi_y = -\frac{x_\eta}{J}, \\ \eta_x &= -\frac{y_\xi}{J}, \quad \eta_y = \frac{x_\xi}{J} \end{aligned} \quad (10)$$

$$\begin{aligned} \xi_t &= \frac{(-x_\tau y_\eta + x_\eta y_\tau)}{J}, \\ \eta_t &= \frac{(x_\tau y_\xi - x_\xi y_\tau)}{J}, \quad \tau = t \end{aligned} \quad (11)$$

where a Jacobian of the coordinate transformation $J = x_\xi y_\eta - x_\eta y_\xi$ and x_τ and y_τ represent moving velocities at each control surface which are

determined using a second-order central difference. The moving wall boundary conditions, when used in the splitting method, can approximately be decomposed into the incompressible and perturbed variables as,

$$\bar{U}_w = \frac{\partial \bar{x}_w}{\partial \tau}, \quad \left. \frac{\partial P}{\partial n} \right|_w = 0 \quad (12)$$

and

$$\begin{aligned} \bar{u}'_w \cdot n &= 0, \quad \left. \frac{\partial \rho'}{\partial n} \right|_w = 0, \\ \left. \frac{\partial p'}{\partial n} \right|_w &= 0 \end{aligned} \quad (13)$$

where n denotes a unit normal vector.

The LPCE is computed in a standard time-marching fashion, whereas the INS is solved by an iterative fractional step method (Poisson's equation for the hydrodynamic pressure). Both the INS and LPCE are solved in a body fitted moving grid system and integrated in time by a four-stage Runge-Kutta method and spatially discretized with a sixth-order compact finite difference scheme [6]. A tenth-order spatial filtering [7] is also applied to every iteration in order to suppress high frequency errors that might be caused by grid non-uniformity. Since the INS and LPCE computations are conducted with different grids for computational efficiency [1-3, 8], a bilinear shape function is used in space to interpolate the source term DP/Dt and hydrodynamic variables onto the acoustic grid. This method maintains sufficient accuracy when interpolation is conducted from fine grid to coarse grid and this is always the case in the present study (hydrodynamic grid: fine, acoustic grid: coarse). For acoustic calculation, an ETA (energy transfer and annihilation) boundary condition [9] with buffer zone is used for

eliminating any reflections of out-going waves at the far-field boundaries.

3. RESULTS AND DISCUSSION

3.1. PHONATION IN HUMAN LARYNX

3.1.1 . Laryngeal flow and sound

In this study, we first explore the relationship between the oscillatory behavior of the vocal folds and the characteristics of the glottal airflow by using an axi-symmetric model [10, 11], which replicates actual movements of the vocal folds during phonation. The laryngeal flow (w_z) and the original sound ($\Delta p'$) within the phonation system are presented in Fig. 1 for one cycle of glottis motions. As the glottis opens like a nozzle, air jet spouts out with vortex shedding at the glottis trailing-edge. On the other hand, the glottis takes a diffuser profile during closure to effectively reduce the flow rate. This time, vortex shedding occurs at the glottis leading-edge like a diffuser stall. The laryngeal flow can be characterized by (i) a pulsating air jet with the local Reynolds number changing in time and (ii) the flow separation point keeps moving back and

forth between the leading- and trailing-edge of the glottis. The latter is specifically related to the rotational motion of the glottis, a unique feature of the glottal motions.

The sound generation processes are described in Fig. 1(b) by the pressure fluctuation field ($\Delta p'$). When the vocal folds are opened, the pressurized air in the subglottal region spouts out and a compression wave is generated and propagates into the supraglottal region (like a piston effect), while a rarefaction wave propagates upstream into the subglottal region. During closure, a volumetric flow rate in the vocal tract becomes minimal with the subglottal pressure being built. At the same time, a rarefaction wave is generated, propagating into the supraglottal region by an isolation effect.

To validate the numerical result, a time variation of the glottal volumetric flow rate is then compared in Fig. 2 with the clinically measured data of Rothenberg [12]. Here, a volume flux within the glottis is computed by integrating an axial velocity across the section in the middle of the glottis ($x = 0$). The predicted volume flow rate agrees reasonably well with the inversely filtered clinical data. Some

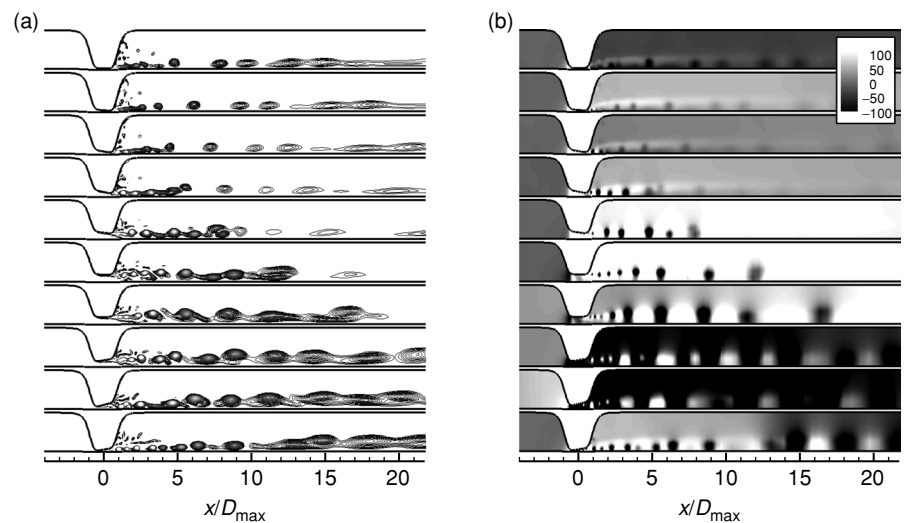


Figure 1. Time evolution of (a) vorticity (50 contours between 0 and 50000) and (b) pressure fluctuation (Pa) (white: compression, black: rarefaction) around the glottis during one cycle.

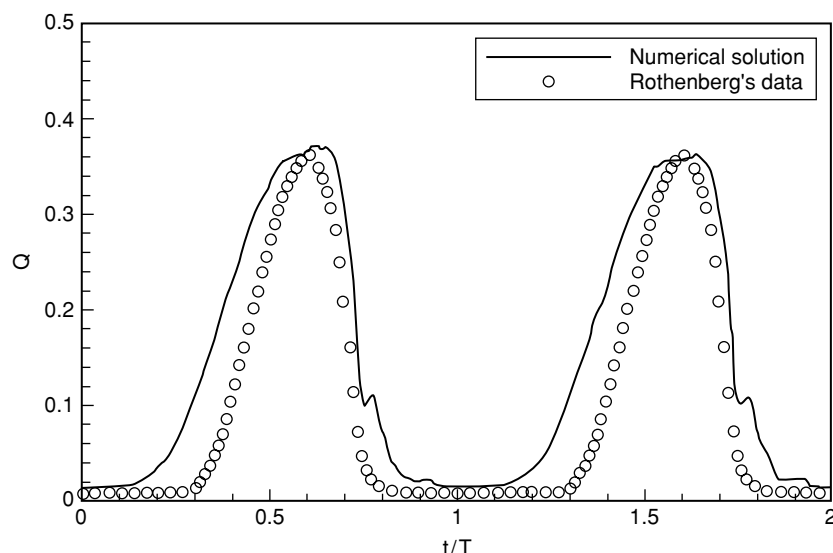


Figure 2. Comparison of glottal volumetric flow rate Q (l/sec); computation (line), clinical (circle).

discrepancies observed at $t/T = 0.1 \sim 0.4$ and $0.6 \sim 0.8$ are due to the fact that an open quotient $Q_0 \{= t_{open}/(t_{open} + t_{close})\}$ is different. Here, t_{open} is a time period, over which the volume flow rate remains constant, while t_{open} is defined as $T - t_{close}$. Q_0 determines the shape of the waveform, regardless of amplitude and period and helps to determine not only the amount of acoustic power but also the sound quality; values lower than 0.4 are associated with a pressed voice and the values above 0.7 tend to have a breathy sound [13]. The value of Q_0 used for computation was approximately 0.7, whereas the clinical data show $Q_0 \approx 0.5$.

3.1.2. Effects of fundamental frequency and rotational motion

In phonation process, there are various glottal properties that make differences between the male and female voices; for example, length, diameter and thickness of the vocal folds. But these glottal properties will eventually make the fundamental frequency different for male and female. So, fundamental frequency is selected to investigate its effects on the characteristics of the laryngeal flow and sound. Figure 3 shows the volumetric flow rates for male

and female, in which f_0 is set to 100Hz and 200Hz, respectively. The male's volumetric flow rate is higher during the glottis opening ($t/T = 0.5$) because the low-frequency glottis motion of the male exerts less resistances to the flow, compared to the high-frequency female case. The male exhibits more pronounced vortical structures in the jet shear layer than the female, and as a result, the male's acoustic pressure is composed of higher frequency components during closure ($t/T = 0.6 \sim 0.8$) due to the stronger vortical interactions within the glottis. The effect of f_0 on voice quality is also shown in Fig. 4 which compares the sound pressure level (SPL) spectra monitored at $(x/D_{max}, r/D_{max}) = (10, 1)$. It is clearly observed that the male's voice is more harsh compared to the female's fluty voice, while the amplitude of the acoustic waves increases with the fundamental frequency because hasty movements of the vocal folds supply more energy to the acoustic waves during phonation. It is also interesting to note that the present computational methods are able to replicate the basic difference of the voice quality, i.e. low-tone brassier voice of male versus high-tone flutier sound of female.

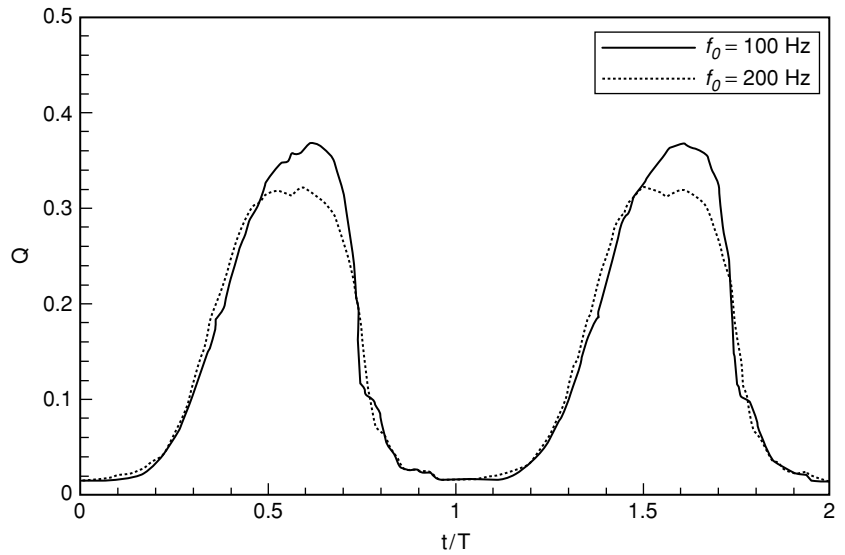


Figure 3. Glottal volumetric flow rate Q (l/sec); male (solid), female (dotted).

Then, we additionally investigate how the rotational motion of the glottis is related to the mechanical efficiency of the glottis as a sound generator, or

the glottal impedance. The glottal impedance, R is defined as a ratio of the pressure difference between the sub- and supra-glottal regions to the

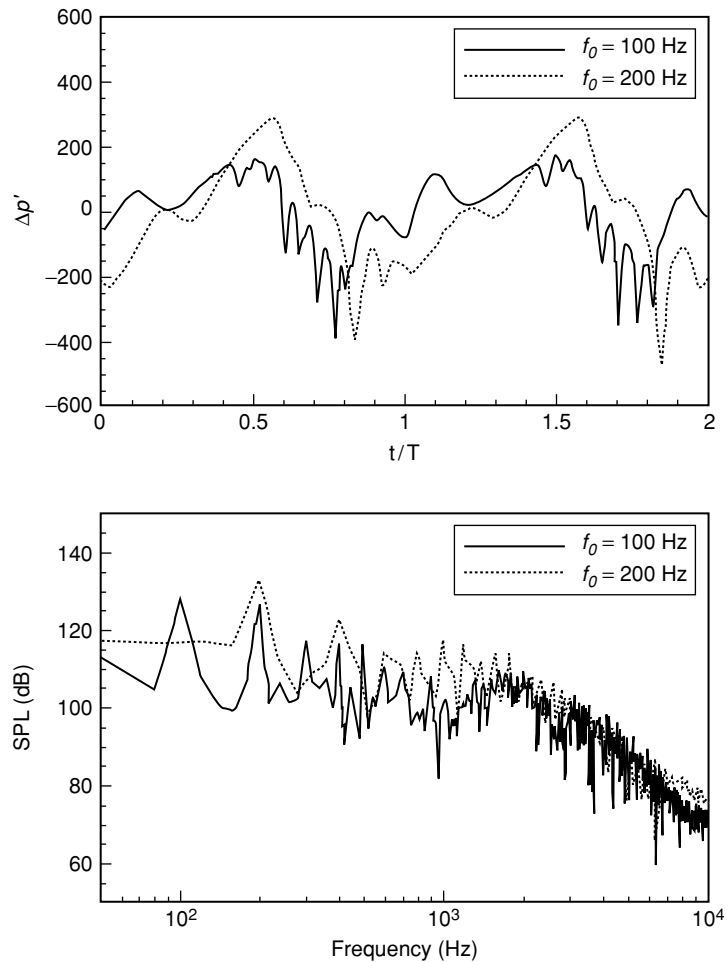


Figure 4. Pressure fluctuation $\Delta p'$ (Pa) at $10D_{max}$ downstream from the glottis and the sound pressure level (SPL) spectra; male (solid), female (dotted).

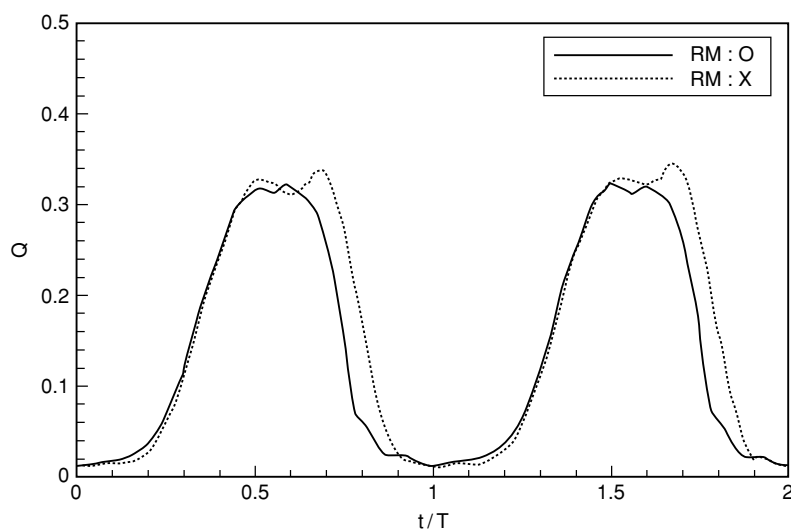


Figure 5. Glottal volumetric flow rate Q (l/sec); rotation (solid), without rotation (dotted).

glottal volume flow rate [13], i.e., $R = \Delta P/Q = (P_{sub} - P_{sup})/Q$ where P_{sub} and P_{sup} are the space-averaged pressures at $x/D_{max} = -2.5$ and $x/D_{max} = 2.5$, respectively. During closure ($t/T = 0.6 \sim 0.8$), the glottis rotates counter-clockwise like a diffuser, causing a flow to be separated at the leading-edge of the vocal cords. As shown in Fig. 5, the rotational motion effectively lowers the glottal volume flow rate Q from 0.24 to 0.1 at $t/T = 0.77$, about -60% more than the case with the translation only. The case is reversed during the glottis opening ($t/T = 1.1 \sim 1.3$). As the glottis rotates clockwise like a nozzle, the separation point moves from the

leading-edge to the trailing-edge and the glottal volume flow rate is consequently increased from 0.018 to 0.026 at $t/T = 1.16$, about +45% more than the case with the translation only. This rotational motion strongly affects the glottal volume flow rate (Q) as well as the glottal impedance (R), as shown in Figs. 5 and 6. So, it is clear that the rotational motion of the glottis controls the glottal impedance by changing the flow separation points between the leading- and trailing-edge of the glottis, and this increases the mechanical efficiency of the glottis as a sound generator in the phonation process, compared to the translation only.

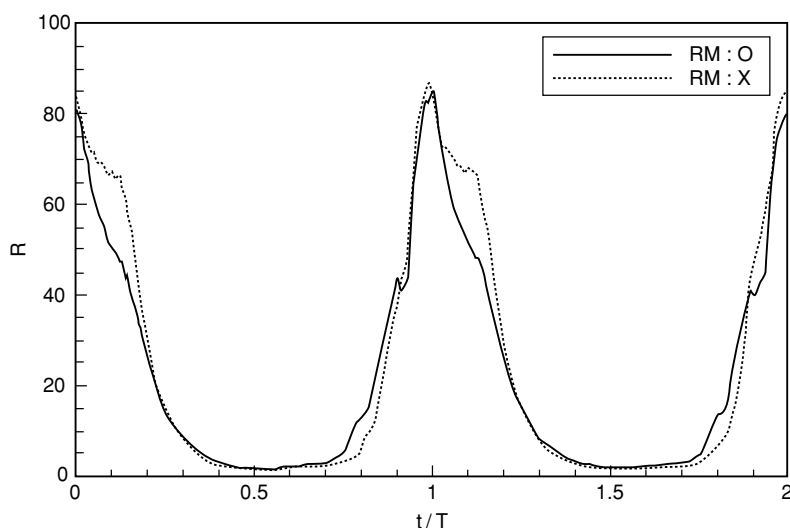


Figure 6. Glottal impedance R ($kPa \cdot sec/l$); rotation (solid), without rotation (dotted).

3.1.3. Effect of glottal closure

The importance of glottal closure is based on the fact that most of the voice disorders are closely related to the abnormalities in the glottis motion [14]. One of the common types is paralysis of one (unilateral) or both (bilateral) of the vocal folds, which is due to the neurological disease such as the Parkinson's disease. Figure 7 shows the effects of glottal closure on the volumetric flow rate. As the opening gap (i.e. minimum diameter of the glottis) increases, the maximum and minimum glottal volume velocities are both increased, representing a greater axial velocity during the glottis closure ($t/T = 4.8 \sim 5.2$). This means that as the vocal fold motion is restricted, i) voice duration is reduced, ii) the pulsating jet becomes weak, and iii) the vortical structures are more pronounced. Therefore, the main dipole sound from the pulsating jet gradually disappears, while the high frequency contributions from the volume sources are more discernable for the cases B, C, and D, as shown in Fig. 8. It follows that when the vocal folds do not vibrate at all (case E),

a dipole sound is no longer present and only the quadruple sound is found downstream.

From a clinical view point, the computational results suggest that a complete glottal closure be needed for fluty sound, clear pitch and sufficient loudness in phonation. On the other hand, if the vocal folds are paralyzed or restricted with small displacements, both pitch and loudness are greatly influenced by the weakening of the pulsating jet, and the voice quality is significantly affected by the vortical interactions within the glottis during the glottis closure. Considering some typical symptoms in disordered phonation [14], the aforementioned acoustic features are quite similar, even though other geometrical effects are not included in the present computations.

3.1.4. Effect of fluid-structure interaction

In reality, a vibratory motion of the vocal folds is self-sustained via a fluid-structure interaction (FSI) process between the elastic body of the larynx and the pulsating air jet within the

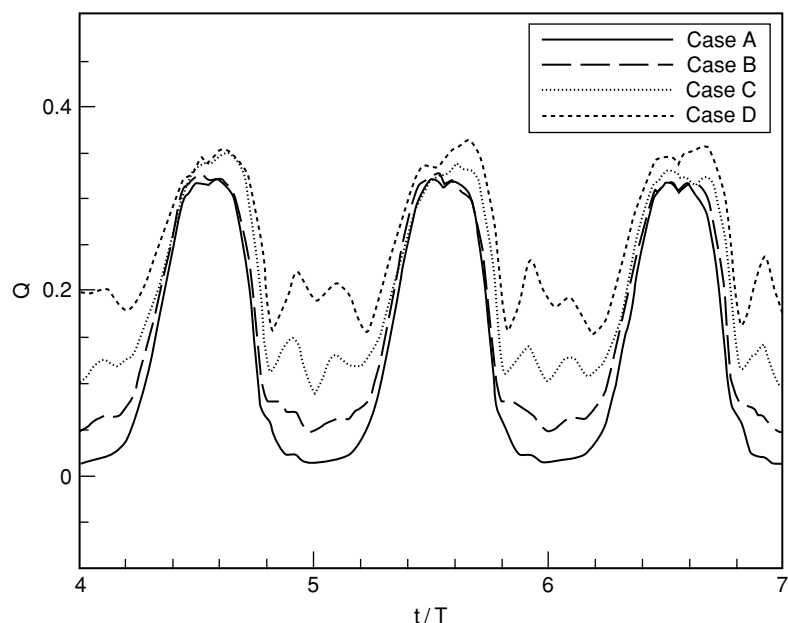


Figure 7. Variation of glottal volumetric flow rates Q (l/sec): minimum diameter of the glottis D_{min} is set to 0.8 mm (Case A), 1.6 mm (Case B), 2.4 mm (Case C), and 3.2 mm (Case D).

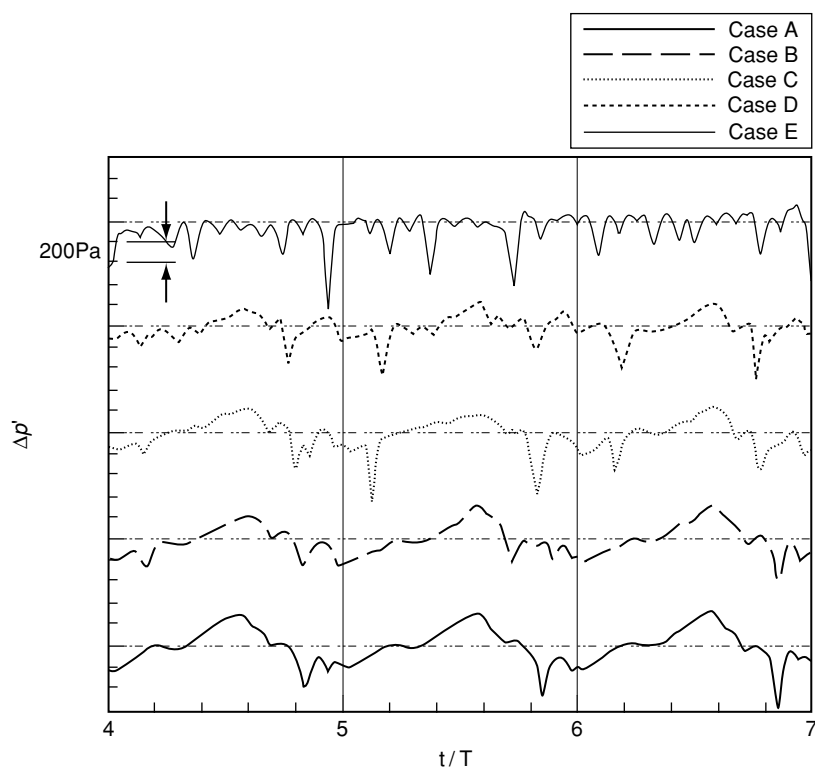


Figure 8. Time history of pressure fluctuations $\Delta p'$ (Pa) at $10D_{max}$ downstream from the glottis: vocal fold does not vibrate at all for Case E, because D_{min} is set to be same with D_{max} .

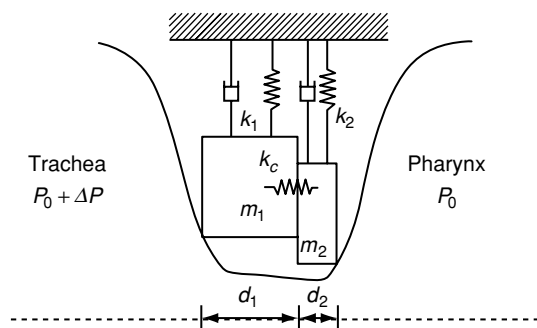


Figure 9. Schematic of low-dimensional vocal fold model: masses and stiffness coefficients are computed through a scaling factor Ψ for easy control of the vocal fold tension, and the details of the model can be found in Reference [15].

glottis. Thereby, reproduction of the flow-induced oscillations is necessary not only for better understanding of the bio-fluid mechanics and the phonation aeroacoustics in the human larynx but also for development of an artificial phonation device. In the present study, we further investigate the effects of bio-mechanical parameters such as glottal width, vocal folds stiffness, and

subglottal pressure on the glottal airflow characteristics as well as on the acoustic features of phonation.

For dynamic control of the vocal folds, which result from the interactions between the pressure and the vocal fold stiffness, the larynx is described again by a low-dimensional body-cover model [15]. Figure 9 depicts a schematic of the vocal fold model. Then, the vocal fold

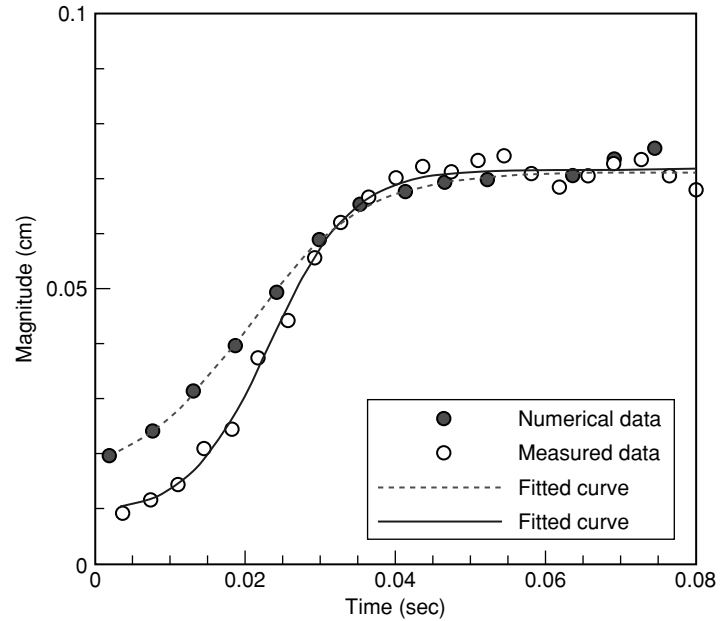


Figure 10. *Magnitudes of vocal folds oscillation at a normal phonation condition.*

vibration is fully coupled with the unsteady flow and sound, which are predicted by a present INS/LPCE splitting method.

Figure 10 shows the dynamic behavior of the vocal fold during phonation. Similar to the previous observations, the growth of the vocal fold amplitudes is found in phonation onset ($t = 0 \sim 0.04$ sec), while the vibration of the vocal fold is self-sustained via FSI process in phonation ($t > 0.04$ sec). It is also shown that both the computed magnitude and the phonation onset time agree well with those of the recorded data for 71 female subjects [16]. Thus it seems that the laryngeal flow and sound as well as the oscillatory behavior of the vocal folds are well predicted by the present computational modeling and FSI procedure.

Then, in order to describe the effects of bio-mechanical parameters, the glottal airflow characteristics as well as acoustic features of phonation are investigated in Fig. 11, where their aerodynamic and aeroacoustic roles are examined with the volumetric flow rate and the sound pressure level (SPL), respectively. As the glottal width increases, the volumetric flow rate

associated with strength of the pulsating jet also increases. As a result, the amplitude of acoustic wave in the vocal tract is increased with the glottal width, while the fundamental frequency $f_0 = 180$ Hz is almost constant (Fig. 11(d)). It is interesting to note that the higher frequency contributions are prominent at initial position $x_0 = 0.14$ cm, because the increase of the local Reynolds number leads to more pronounced vortical structures in the jet shear layer. The subglottal pressure DP plays an important role on reproduction of the self-sustained oscillation of vocal folds. As shown in Fig. 11(b), subglottal pressure greater than a certain threshold pressure P_{th} is essential for maintenance of the vocal fold vibrations during speech. In the present computation ($x_0 = 0.15$ cm), P_{th} is estimated about 700Pa, which is close to the value of Titze [13]. If ΔP is larger than P_{th} , self-sustained oscillation occurs, leading to greater contribution of the fundamental frequency in SPL spectrum. On the other hand, at lower ΔP , the pulsating jet becomes weak so that the main dipole sound gradually disappears (Fig. 11 (e)). In addition, the effect of a scaling factor which controls the degree of tension is shown in Figs. 11(c) and

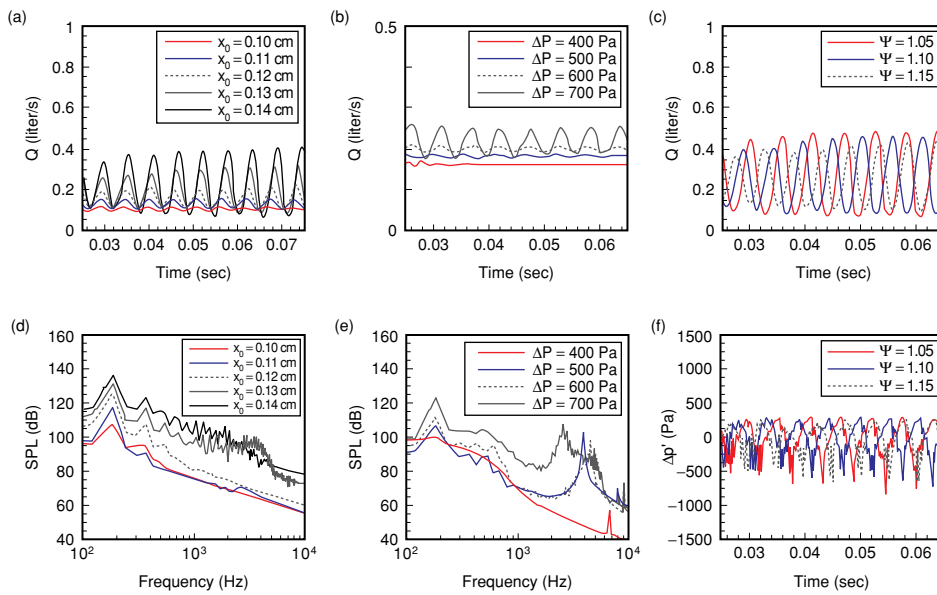


Figure 11. Temporal variations of the volume flow rate (a, b, and c) and SPL spectra (d, e, and f) at $z = 40 D_{max}$

11(f). As expected, the fundamental frequency f_0 can be regarded as a function of vocal fold tension, i.e. the greater tension, the higher fundamental frequency. It is also worthy noting that SPL and frequency composition do not vary significantly by increase of Ψ , implying that a voice quality is mainly affected by the glottal width and subglottal pressure rather than vocal fold stiffness.

3.2. A BUZZ SOUND OF BUMBLEBEE

3.2.1. Aerodynamics of flapping wing

A flapping motion of the insect wing has many intriguing features for biologists, physicists, and engineers. For example, highly efficient flight performance of insects has fascinated engineers who are interested in developing a micro-mechanical flying insect (MFI) based on bio-mimetic principles. With this respect, a great deal of experimental [17–19] and numerical [20–22] studies have been conducted to understand the high-lift mechanism of the insect flight. On the contrary, the aerodynamic sound of flying insects has received less

attention, although its acoustic characteristics and the associated generation mechanisms are important not only for the fundamental studies of insect physiology and evolution but also for their bio-mimetic applications. Thereby, we investigate how the flapping wing sound or so-called ‘buzz’ sound is generated during the flight, providing more comprehensive explanations on the radiation pattern and sound generation mechanisms associated with the flapping wing sound [23].

First, the flow and sound fields are computed for the two-dimensional modeled wing in hovering motion. Figure 12 shows the time evolution of the computed vorticity field around the wing for the first half cycle of the hovering motion. In the transverse motion ($t/T = 1/10 \sim 2/10$), the leading and trailing-edge vortices are generated in large scale. During tangential motion ($t/T = 3/10 \sim 4/10$), the eddies shed from the leading-edge scatter at the trailing-edge, and at the end of the downstroke ($t/T = 5/10$), the rotational motion lets the leading-edge vortex to be swept away from the wing so that the dipole vortices

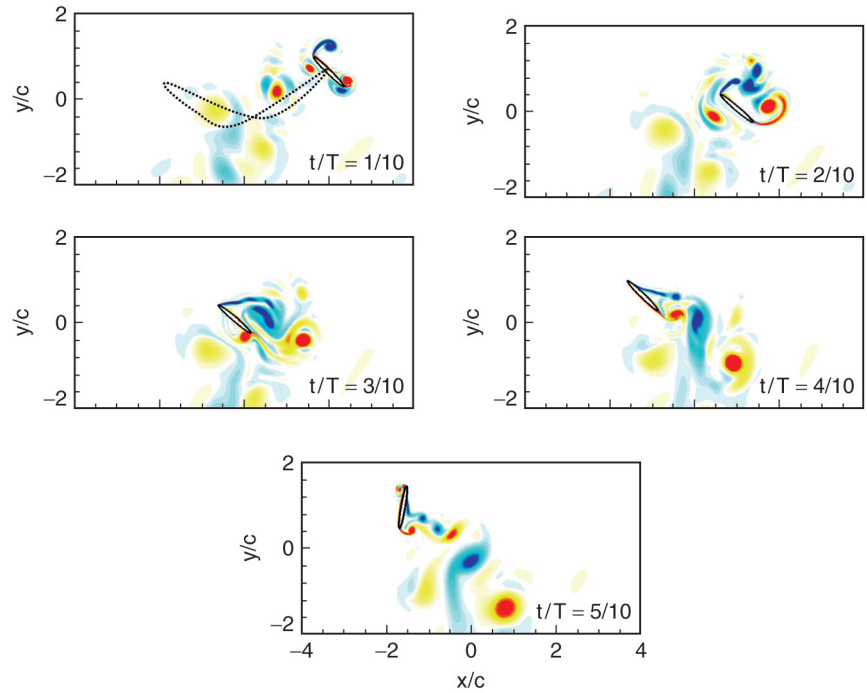


Figure 12. Time evolution of vorticity fields around the flapping wing in down-stroke at hovering. $T = 1/f$ denotes a period and the black dotted line indicates the stroke path.

move downward by themselves due to their induced velocity fields. This process is repeated in another half cycle. It is interesting to note that the co-moving vortices created in the previous downstroke (or upstroke) do not interfere with the formation of the vortices during another half cycle because they are already out of the stroke path. The time variations of the drag and lift coefficients of the flapping wing are also presented in Fig. 13. It is indicated that the mean drag coefficient (averaged over 10 periods) is nearly 0, while the

mean lift coefficient is about 0.66. From the definition of $C_L = F_L/0.5\rho_0 U_{max} cR$, one can calculate the lift force on a three-dimensional wing, employing the properties of the bumblebee [24]. Typically, the maximum translational velocity U_{max} of the bumblebee is 17m/s so that the lift force generated by a pair of 3D wing is about 3.11×10^{-2} N. This value is large enough to support the weight of bumblebee, 8.63×10^{-3} N, although the three-dimensional effects neglected in this study could partially reduce the lift force.

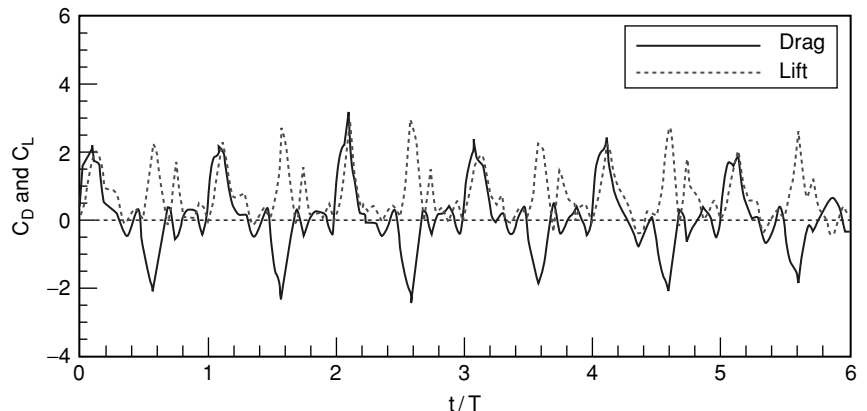


Figure 13. Time history of drag and lift coefficients during hovering.

3.2.2. Sound generation mechanism

The sound fields of the flapping wing in hovering motion are presented in Fig. 14. The computed results indicate that the flapping wing sound is generated by two different basic mechanisms. First, a dipole sound is generated by the transverse motion of the wing (Fig. 14(a) and 14(b)). Due to the fact that the dipole axis changes its direction from downstroke to upstroke, a drag dipole is generated at wing beat frequency ($St = fc/c_0 = 0.004$), while the lift dipole is produced at $2f$ (i.e. $St = 0.008$),

similar to the drag and lift coefficients. Hence, the flapping wing sound is directional. As shown in Fig. 15, the sound pressure level (SPL) peak corresponding to the lift dipole ($St = 0.008$) is not present or weak at 0° and 180° , while the wing beat frequency (drag dipole) is also not present at 90° and 270° . At other angles, both the drag and lift dipoles clearly exhibit their peaks. This result is similar to the previous observation by Sueur *et al.* [25], indicating that the wing beat frequency is most dominant in the front, whereas

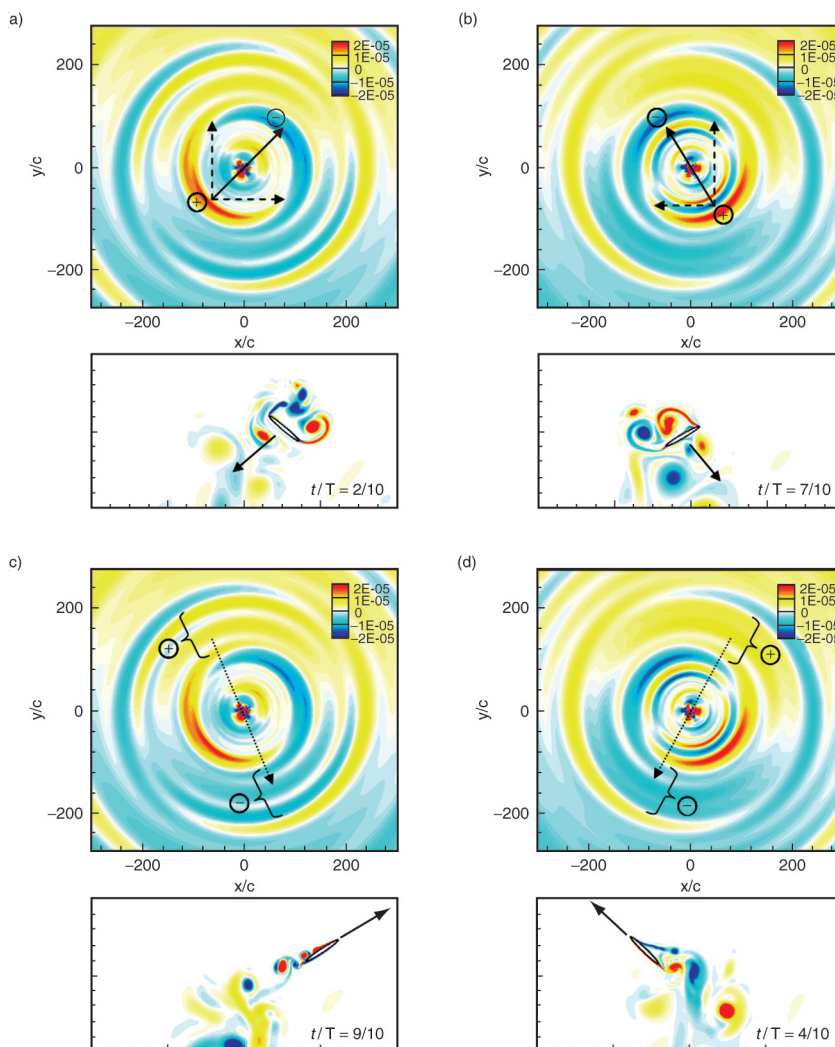


Figure 14. Top: instantaneous pressure fluctuation $\Delta p'$ contours around the wing in hovering motion at $t/T = 0.5$ for (a) and (c) and at $t/T = 1$ for (b) and (d). The pressure fluctuations are normalized by ρc_0^2 where c_0 is the speed of sound. Bottom: hydrodynamic flow fields representing the associated sound sources: (a) and (b) wing loading by transverse motion, (c) and (d) vortex edge-scattering during tangential motion.

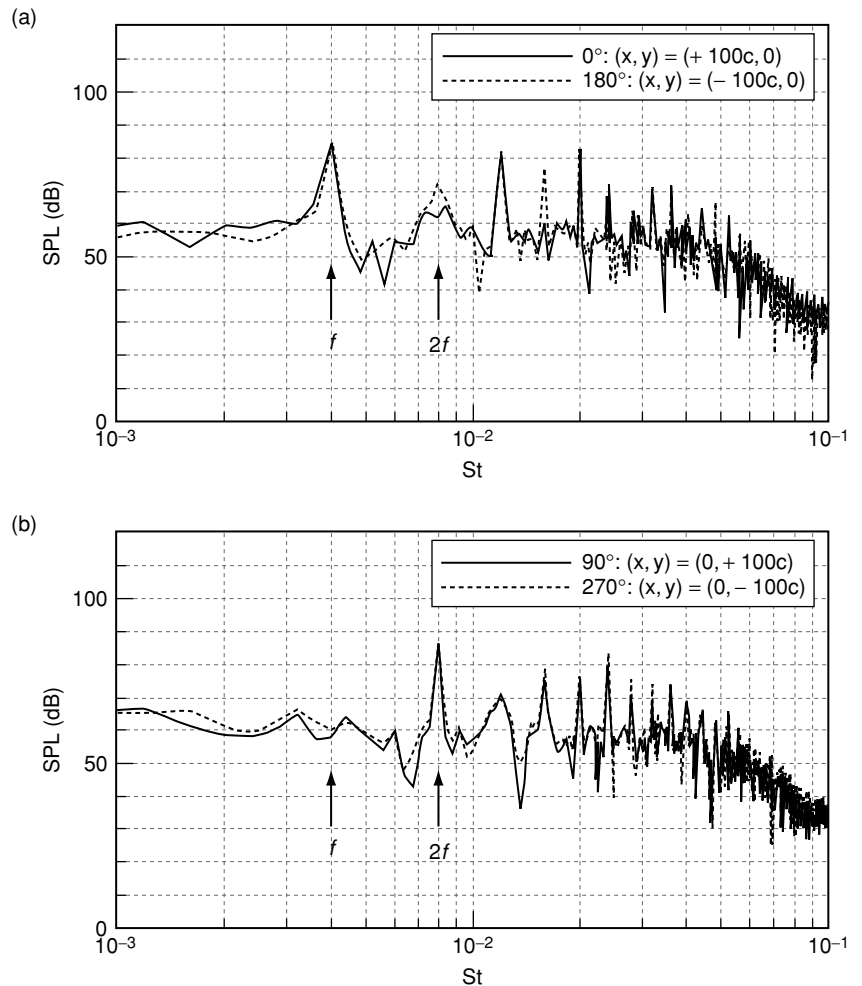


Figure 15. Sound pressure level spectra of flapping wing in hovering motion; (a) horizontal direction at $(\pm 100c, 0)$ and (b) vertical direction at $(0, \pm 100c)$.

the second harmonic is most appreciable at sides.

Another sound source is associated with vortex edge-scattering during tangential motion of the wing. In Fig. 14(c) and 14(d), one can identify the sound waves (bracketed) at $150c \sim 175c$ from the center with wavelengths (λ) observed as $41c$ and $48c$ at $t/T = 0.5$ and 1 , respectively. Considering the wave speed c_0 ($= 340 \text{ m/s} = 250c/T$), the travel time of the waves is estimated as $0.6 \sim 0.7$ (i.e. $\Delta t/T = 150/250 \sim 175/250$). So, it is figured that these waves were generated during $t/T = 8/10 \sim 9/10$ and $3/10 \sim 4/10$ at each stroke. Now, one can note that the flow fields at $t/T = 9/10$ and $4/10$ clearly exhibit the vortical structures that are responsible for

producing the dipole sound during tangential motion of the wing. The vortices in the shear layer emanated from the leading-edge scatter at the trailing-edge of the wing and generate waves radiating perpendicularly to the wing. It is also found that the frequencies of these waves are close to $St (= fc/c_0 = c/\lambda) = 1/48 \sim 0.02$ and $1/41 \sim 0.024$. The above frequencies of dipole tones generated at the trailing-edge agree fairly well with the theory on shear layer instability [26]. Finally, one can note in the spectrum that the SPL peaks are multiples of wing beat frequency with comparable amplitudes (Fig. 15). This frequency composition closely resembles the buzz sound of fly measured by Sueur et al. [25].

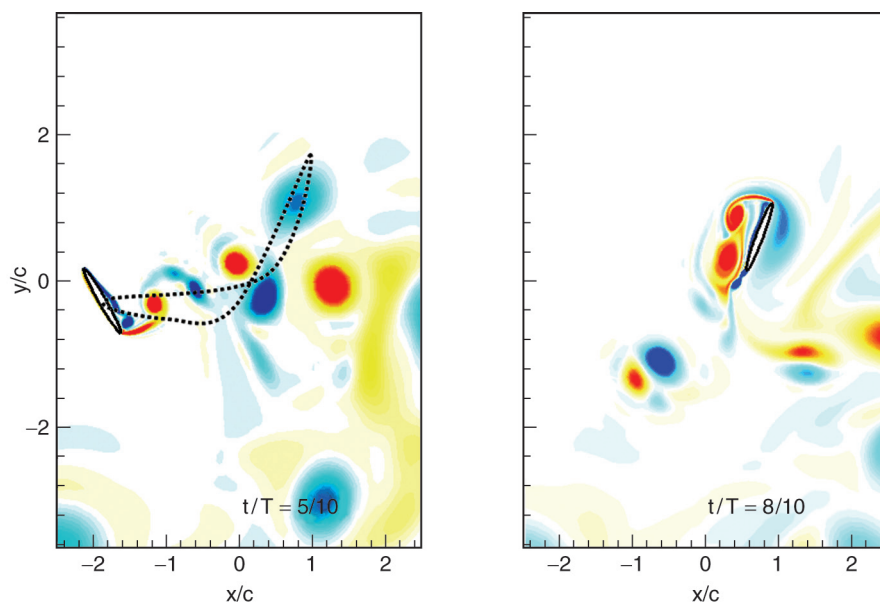


Figure 16. Time evolution of vorticity fields around the flapping wing at forward flight. The black dotted line indicates the stroke path of the forward flight.

3.2.3. Effect of flight condition

Now, we consider the flow and sound fields for the flapping wing in forward flight. Figure 16 shows the vortical structure around the wing at forward flight condition of bumblebee. Due to the free stream effect, the vortices shed from the leading and trailing-edge of the wing during transverse motion are not developed as symmetric as for the hovering case and so are the induced velocity fields. Therefore, these vortices cannot self-propel away from the wing but rather remain in the stroke paths, as

shown in Fig. 16. Besides, the ratio between the free stream velocity and the maximum translational velocity of the wing is close to 0.26 and so the convection effect is quite weak. As a result, the vortices drifting around the flapping wing encounter complex wing-vortex interactions. When compared with the hovering case, this clear distinction in vortical flow structure is expected to change the aerodynamic sound characteristics for the forward flight case. The directivity shown by drag and lift dipoles from wing loading

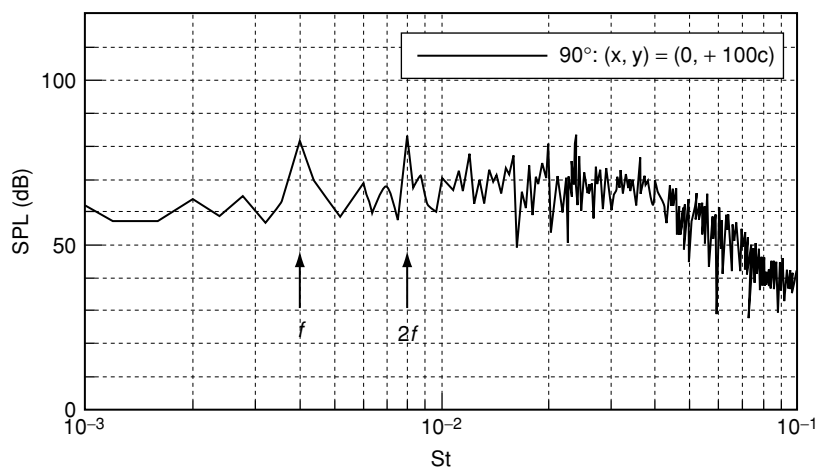


Figure 17. A representative SPL spectrum around the flapping wing in forward flight; similar frequency compositions are found in all directions.

disappears. One may also note that the dipole tones generated at the trailing-edge ($St = 0.02$ and 0.024) are not as distinct as for the hovering case (Fig. 17). These are largely due to the prominent interactions between wing and vortices, being considered as a discernible difference in acoustic feature between the hovering and the forward flight conditions.

4. CONCLUSION

In this study, it is demonstrated that the proposed INS/LPCE hybrid method can efficiently predict the bio-fluid sounds, in which compressibility effects are not so strong but important biologically. For the human larynx and the flapping wings of bumblebee, some characteristic features of the motions were explained in association with their particular sound generation processes. In the future study, a new method is still to be explored to handle the complex geometries such as nasal cavities, lung airways, etc., in which not only flow but also its sound fields are needed to be resolved with accuracy.

REFERENCES

- [1] Seo, J.H. and Moon, Y.J., Linearized Perturbed Compressible Equations for Low Mach Number Aeroacoustics, *Journal of Computational Physics*, 2006, 218, 702–719.
- [2] Seo, J.H. and Moon, Y.J., Perturbed Compressible Equations for Aeroacoustic Noise Prediction at Low Mach Numbers, *AIAA Journal*, 2005, 43, 1716–1724.
- [3] Moon, Y.J. and Seo, J.H., A Splitting Method for Aeroacoustic Noise Prediction of Low Mach Number Viscous Flows, *International Journal of Aeroacoustics*, 2005, 4(1), 1–16.
- [4] Chang, K.W., Seo, J.H., Moon, Y.J. and Roger, M., Prediction of Flat Plate Self-Noise: Proceedings of the 12th AIAA/CEAS Aeroacoustics Conference, AIAA Paper 2006–2513, 2006.
- [5] Seo, J.H. and Moon, Y.J., Aerodynamic Noise Prediction for Long-Span Bodies, *Journal of Sound and Vibration*, 2007, 306, 564–579.
- [6] Lele, S.K., Compact Finite Difference Schemes with Spectral-Like Resolution, *Journal of Computational Physics*, 1992, 103, 16–42.
- [7] Gaitonde, D., Shang, J.S. and Young, J.L., Practical Aspects of High-Order Numerical Schemes for Wave Propagation Phenomena, *International Journal for Numerical Methods in Engineering*, 1992, 45, 1849–1869.
- [8] Seo, J.H. and Moon, Y.J., Prediction of Low Mach Number Turbulent Flow Noise using the Splitting Method: Proceedings of the 10th AIAA/CEAS Aeroacoustics Conference, AIAA-Paper 2004–2860, 2004.
- [9] Edgar, N.B. and Visbal, M.R., A General Buffer Zone-Type Non-Reflecting Boundary Condition for Computational Aeroacoustics: Proceedings of the 9th AIAA/CEAS Aeroacoustics Conference, AIAA-Paper 2003–3300, 2003.
- [10] Zhao, W., Zhang, C., Frankel, S.H. and Mongeau, L., Computational Aeroacoustics of Phonation, Part I: Computational Methods and Sound Generation Mechanisms, *Journal of the Acoustical Society of America*, 2002, 112, 2134–2146.
- [11] Bae, Y. and Moon, Y.J., Computation of Phonation Aeroacoustics by an INS/PCE Splitting Method, *Computers & Fluids*, 2008, 37, 1332–1343.
- [12] Rothenberg, M., The Glottal Volume Velocity Waveform during Loose and Tight Voiced Glottal Adjustments: Proceedings of the 7th International Congress of Phonetic Sciences, 1971.
- [13] Titze, I.R., *Principles of Voice Production*, Prentice Hall, New Jersey, 1994.
- [14] Boone, D.R., McFarlane, S.C. and von Berg, S.L., *The Voice and Voice Therapy*, Allyn & Bacon, Boston, 2005.

- [15]Lucero, J.C. and Koenig, L.L., Simulations of Temporal Patterns of Oral Airflow in Men and Women using a Two-Mass Model of the Vocal Folds under Dynamic Control, *Journal of the Acoustical Society of America*, 2005, 117, 1362–1372.
- [16]Braunschweig, T., Flaschka, J., Schelhorn-Neise, P. and Döllinger, M., High-Speed Video Analysis of the Phonation Onset, with an Application to the Diagnosis of Functional Dysphonias, *Medical Engineering & Physics*, 2008, 30, 59–66.
- [17]Ellington, C.P., van den Berg, C., Willmott, A.P. and Thomas, A.L.R., Leading-Edge Vortices in Insect Flight, *Nature*, 1996, 384, 626–630.
- [18]Birch, J.M. and Dickinson, M.H., Spanwise Flow and the Attachment of the Leading-Edge Vortex on Insect Wings, *Nature*, 2001, 412, 729–733.
- [19]Dickinson, M.H., Lehmann, F.O. and Sane, S.P., Wing Rotation and the Aerodynamic Basis of Insect Flight, *Science*, 1999, 284, 1954–1961.
- [20]Wang, Z.J., Two Dimensional Mechanism for Insect Hovering, *Physical Review Letters*, 2000, 85, 2216–2219.
- [21]Sun, M. and Tang, J., Unsteady Aerodynamic Force Generation by a Model Fruit Fly Wing in Flapping Motion, *Journal of Experimental Biology*, 2002, 205, 55–70.
- [22]Sun, M. and Tang, J., Lift and Power Requirements of Hovering Flight in *Drosophila*, *Journal of Experimental Biology*, 2002, 205, 2413–2427.
- [23]Bae, Y. and Moon, Y.J., Aerodynamic Sound Generation of Flapping Wing. *Journal of the Acoustical Society of America*, 2008, 124(1), 72–81.
- [24]Weig-Fogh, T., Quick Estimates of Flight Fitness in Hovering Animals, Including Novel Mechanism for Lift Production, *Journal of Experimental Biology*, 1973, 59, 169–230.
- [25]Sueur, J., Tuck, E.J. and Robert, D., Sound Radiation Around a Flying Fly, *Journal of the Acoustical Society of America*, 2005, 118, 530–538.
- [26]Blake, W.K., *Mechanics of Flow-Induced Sound and Vibration* (vol. 1), Academic Press, Orlando, 1986.

GARDENER THREATENED OVER LEAF BLOWER NOISE

Redondo Beach (California) resident was booked into jail April 28 after allegedly threatening to shoot his neighbor's gardener for making too much noise with a leaf blower. Martin Monahan, 51, "said he was going to shoot the victim if he continued to use the lawn blower," police spokesman Sgt. Phil Keenan said. When police arrived, Monahan surrendered peacefully, according to the Redondo Beach Police Department. Monahan was booked on suspicion of making a criminal threat, and was being held on \$50,000 bail.

GLASWEGIAN IGNORE CAR ALARMS

A car alarm is more likely to be ignored in Glasgow than in any other major city of the UK, an insurance company has suggested. The few Glaswegians who did react to an alarm during "tests" were unlikely to contact police, according to Aviva. The company said it conducted tests in Glasgow, London, Cardiff and Manchester, gauging how people responded to a car's alarm being set off in the street. Glasgow was found to have the greatest level of "alarm apathy", with 91% of passers-by showing no sign of being aware of the noise at all. The test involved sounding a car alarm for an hour in the Clarkston area in the city's southside. In that time, 22 people walked past the car, of whom only two showed signs of acknowledging the sound. Of the 115 people tested across the four cities, not one of them investigated the noise or reported possible criminal activity. People in Cardiff were the most alert: a quarter of those tested paid some attention to the car alarm, Aviva said. Martin Smith, motor claims manager at Aviva, said: "Alarms obviously offer a straightforward method for protecting a car and it's important that, where possible, cars are fitted with them. But it's clear from our research that they've become like urban white noise, as commonplace as dogs barking, sirens and everyday traffic."

TURBINES DON'T HARM HEALTH, EXPERTS SAY

Living near wind turbines doesn't cause serious harm to human health, two experts for Suncor Energy have testified at a hearing in Chatham, Ontario. Epidemiologist Kenneth Mundt from a Massachusetts consulting firm ENVIRON reviewed literature on wind turbines and concluded the epidemiological evidence to date is not sufficient to support the statement that wind turbine exposure causes harm to human health. Christopher Ollson of Stantec consulting, who was called as an expert in environmental health, said his review of literature also found living near a wind turbine would not result in serious harm to health. During his testimony Ollson said annoyance from the noise of wind turbines is a health effect. "What I'm not suggesting is that that is equivalent to serious harm to health," he said. The two were testifying at a hearing of Ontario's Environmental Review Tribunal. The case is being watched across Ontario and has been called precedent-setting because Suncor's Kent Breeze Wind Farm west of Thamesville was the first to receive a renewable energy approval under the Green Energy Act. It was also the first to be appealed under the act when Chatham-Kent Wind Action Inc. and resident Katie Erickson appealed based on issues of harm to human health from noise and low-frequency sound. In February, Dr. Robert McMurtry, a former dean of the University of Western Ontario's medical school and a former assistant deputy minister of health for the federal government, testified that wind turbine construction should be put on hold until medical studies are done. He told the hearing of people who lived near wind turbines and complained of not being able to sleep, stress, headaches and high blood pressure. At the hearing, Eric Gillespie, the lawyer for the Chatham-Kent Wind Action group, challenged part of epidemiologist Mundt's testimony. Gillespie said Mundt had quoted from a Health Canada document from 2005 that said the common effect of community noise is annoyance but that he didn't quote the rest of the sentence which said noise is considered an adverse health effect by the World Health Organization. Mundt said he didn't include it because he couldn't substantiate it.